Supercritical water injection in a single cylinder research engine: a PIV study

Supercritical water injection in a single cylinder research engine: a PIV study

M Piras[1,2], L Marchitto[2], C Tornatore[2]

[1] Industrial Engineering Department, Mechanic and Energetic Section, University of Naples "Federico II", via Claudio 21, 80125, Naples, Italy
[2] STEMS/CNR, Italian National Research Council, Via Marconi 4, 80125, Naples, Italy

marco.piras@unina.it

M Piras: https://orcid.org/0000-0003-2710-4662
L Marchitto: https://orcid.org/0000-0003-3834-3992
C Tornatore: https://orcid.org/0000-0001-9460-0549

Abstract. This work presents the experimental results of a fluid dynamic investigation to characterize the injection of supercritical water in the combustion chamber of an internal combustion engine. Particle Image Velocimetry (PIV) analysis is carried out in an optically accessible 2-stroke Diesel engine. A prechamber, equipped with two optical accesses is connected to the main cylinder through a tangential duct so that the piston stroke induces a swirled motion field with angular velocities typical of light duty engines for automotive application. The engine is equipped with an injection system for the production and injection of supercritical water, with the possibility to independently regulate the injection pressure, temperature, duration, and timing. Tests have then been carried out under different operating conditions to evaluate the impact of the fluid dynamics in the combustion chamber on the water spray. First, the airflow velocity field has been characterized at different engine crank train angles. The water spray has been macroscopically characterized for an injection temperature of 300°C and pressure of 30Mpa. Then, the supercritical water/air interaction has been explored, at different injection pressure, temperature, and Start of Injection (SOI) to provide global information in terms of spray morphology, tip penetration, and velocity vector distribution of the water droplets within the combustion chamber for different injection strategies.

1. Introduction

Despite the growing interest in electric vehicles and other alternative forms of propulsion, internal combustion engines (ICEs) continue to dominate the transportation sector. In fact, according to recent statistics, over 90% of the world's transportation still relies on ICEs [1]. Further, full electric propulsion is unfeasible for applications where battery recharge is prevented or difficult (i.e. marine transportation, mining, agriculture etc.). As such, ICEs remain a critical technology for meeting global transportation needs, and their development and optimization are essential to achieve energy security, reduce emissions, and improve fuel efficiency. Spark-ignition engines require knock mitigation to increase their efficiency reducing CO_2 emissions. Various techniques have been

proposed and analyzed in the literature to prevent knock occurrence. The Miller cycle, implemented through Late Intake Valve Closure or Early Intake Valve Closure, is a widely used strategy that can effectively reduce knock propensity [2–5]. External cooled Exhaust Gas Recirculation (EGR) circuits have also been extensively studied for knock mitigation in current literature [6–10]. Water injection is another promising solution, as it cools the in-cylinder charge through its large latent heat of vaporization. Unlike EGR gas, water vapor has a thermal action that suppresses knock and reduces NOx emissions [11–16]. In addition, water can be used as a flow to recover energy from exhaust gases. In fact, despite the advancement of modern technologies, approximately 50% of the energy released through combustion in Internal Combustion Engines (ICEs) is lost to the environment through the cooling system and exhaust gases. These energy losses significantly affect the efficiency of ICEs. Therefore, an additional key to achieves a significant improvement in ICE efficiency and performance lies in the recovery of exhaust and cooling energy. Cantiani et al. proposed utilizing exhaust gas energy to increase water temperature above its critical value and introduce supercritical water (SCW) directly into the chamber during the final stages of the combustion process. This method increases in-cylinder pressure and improves the engine cycle's work output. Moreover, lowering the in-cylinder temperature reduces the rate of wall heat transfer. The injection of water under supercritical conditions is advantageous as it avoids the pressure drop associated with the latent heat of vaporization, which typically decreases efficiency [17,18]. The water-air interaction is a critical aspect to fully understand the effect of the SCW injection on the in-cylinder turbulence. The utilization of planar particle image velocimetry (PIV) technique has facilitated the measurement of instantaneous air velocities, and the calculation of spatial derivative properties. In [19] PIV measurements have been applied to study mixture entrainment process of torch flames typical of prechamber engines. Results showed that the air entrainment rate is directly proportional to the injection pressure. Tsiogkas et al. [20] used PIV to measure cold flows in an optical internal combustion engine during the intake phase at 1000 and 1500 rpm engine speed. They found that the maximum flow velocity at 1500 RPM is higher as compared to 1000 RPM for every CAD at tumble plane and a counter-clockwise tumble motion was observed during both at 1000 and 1500 RPM. The objective of the present paper is to investigate the effects of SCW injection in an optically accessible diesel engine and analyse the impacts of different injection strategies.

2. Engine and operating conditions

Engine test bench includes a single cylinder 2-stroke optically accessible Diesel engine equipped with a common rail high pressure injection system, a supercritical water injection system and a swirled combustion chamber. The engine main characteristics are reported in Table 1. The cylindrical shaped combustion chamber has a diameter of 50mm and a depth of 30mm. It is connected to the main cylinder through a tangential duct, enabling air flow to enter the chamber during the compression stroke. This generates a counter-clockwise swirl flow within the chamber, with the rotation axis approximately coincident to the symmetry axis of the chamber. This unique design has the aim to reproduce a fluid dynamic environment similar to that of a real direct injection diesel engine. The fuel injector is mounted within the swirled chamber and is oriented with its axis coincident to the chamber axis, allowing for the fuel to mix with the swirling air flow. A sketch representing the cross section of the engine combustion chamber is shown in Figure 1 (left). A further access on the top of engine head has been used to install the water injector, mounted at 90°C respect to the diesel one; Figure 1 (right) shows the experimental set-up.

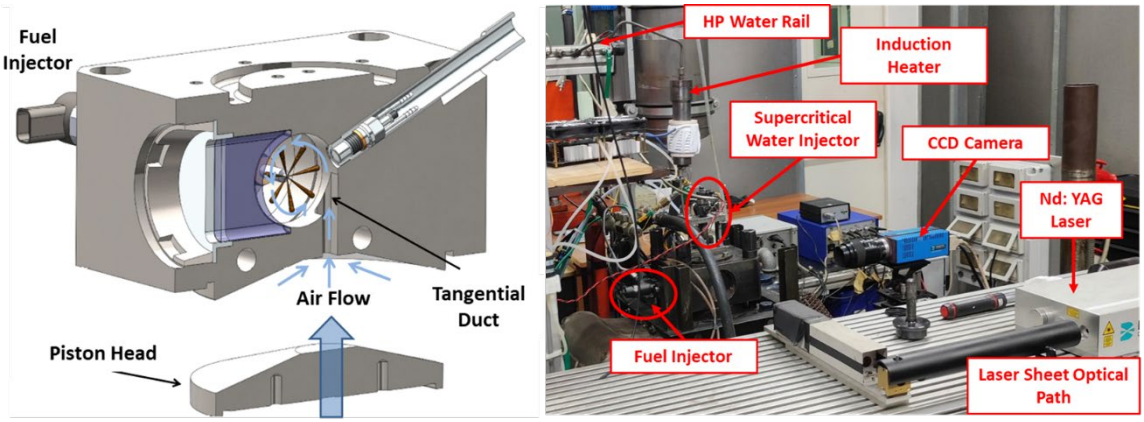

Figure 1. Sketch of the cross section of the optically accessible combustion chamber (left) and picture of the experimental set-up

Table 1. Engine specifications.

Bore	150 mm
Stroke	170 mm
Connecting Rod	360 mm
Compression ratio	10.1:1
Air supply	Roots blower

The combustion chamber has a circular optical access of 50 mm diameter and a rectangular one (size of 10 × 50 mm^2) at 90°, which is used for laser illumination input. The common rail diesel injection system is equipped with a solenoid-controlled injector with 7-hole, 0.12 mm nozzle for automotive applications.

A scheme of the SCW injection system is reported in Figure 2. A low-pressure pump (up to 6 bar) feeds a high-pressure piston pump with distilled water stored in a tank. In this way cold water can be pressurized up to 500 bars in a high-pressure rail typical of diesel engines applications. The rail is then followed by a prototypal induction heater, (equipped with two K thermocouples to measure its surface and water's temperature at the heater outlet) that can heat up the water up to 500°C. All the tests have been performed at the engine speed of 500 rpm with the aim of investigating the effects of water injection pressure, injection temperature and start of the injection on the flow field in the combustion chamber. Table 2 reports the main parameters set for the water injection strategies. The injection duration has been set to 0.5 CAD (corresponding to ≃ 165 μs) to avoid water in oil dilution inside the engine and to get good droplets distribution within the combustion chamber for PIV processing.

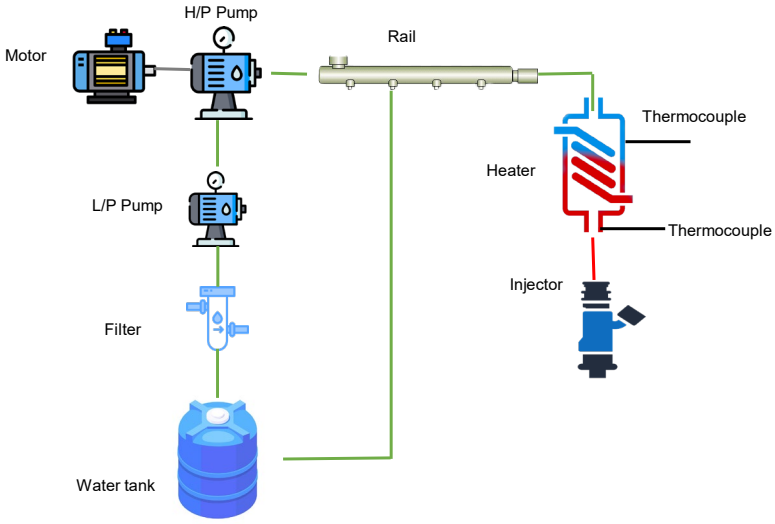

Figure 2. Supercritical water injection system scheme.

Diesel fuel droplets have been used as seeding particles for PIV measurements only for preliminary tests to characterize the air flow velocity distribution in the absence of water injection at different time instants. In these cases, a small amount of fuel (about 1 mg) has been directly injected into the combustion chamber at -60 CAD ATDC. As discussed in [21], the choice of diesel as a tracer is justified by the diesel droplets' capability to follow the flow. The AVL INDICOM, driven by an optical encoder with a resolution of 0.2 crank angle degrees (CAD), was employed to collect data during combustion engine tests. To measure the pressure in the swirl chamber, an AVL QC34C quartz pressure transducer was utilized.

Table 2. Water injection strategies specifications.

TEST #	**1**	**2**	**3**	**4**	**5**	**6**	**7**	**8**
P_{inj}, MPa	25	30	25	25	25	30	30	30
T_{inj} ,°C	420	420	400	420	465	430	430	430
SOI, CAD ATDC	0	0	0	0	0	0	10	20
DOI, CAD	0.5	0.5	0.5	0.5	0.5	0.5	0.5	0.5

3. PIV methodology

The PIV system consists of a twin head pulsed Nd: YAG laser, which contains two independent lasers operating at their second harmonic (532 nm), a CCD camera, and a synchronizer, all used for air flow and droplet images acquisition. The laser beam is shaped into a 0.1mm thick and 50mm high sheet using a series of spherical and cylindrical lenses. The CCD camera collects the scattered light from the spray and works in double shutter mode for PIV acquisition, providing couples of 2048×2048 pixels images with a resolution of 14 bits and a pixel size of 7.4×7.4 μm^2. The first frame is controlled in exposure, the second one has a fixed period equal to the readout time of the first image, whose interval is 68 ms. The CCD camera is aligned at an angle of 90° to the laser sheet. It is connected to a frame

grabber and controlled by a synchronizer that also activates the Nd:YAG laser. To collect PIV images at different injection times, an engine timing unit (ETU) triggers the PIV synchronizer and the electronic control unit (ECU) of the injection system. The images were taken by aligning the light sheet to a plane parallel to the water injector axis and located near the nozzle tip. The optical set-up provided a scale factor of 3.602. The data were collected with a 1.7μs delay between the light pulses and processed using the adaptive correlation method with a final interrogation region of 32×32 pixels. By using a method that utilizes an initial interrogation area (IA) with a size N times larger than the final IA, this approach leverages the intermediate results as information for the subsequent IA of smaller size, until the final IA size is achieved. Starting from a size of 128×128 pixels, the final IA size of 32×32 pixels was attained using this approach. In order to exclude the region outside the combustion chamber from the data processing, a mask has been utilized to filter the images. By implementing this technique, the information collected and analyzed is limited to the relevant areas within the combustion chamber, thus increasing the accuracy and effectiveness of the data analysis. To ensure the accuracy of the results, a "Mooving average validation" has been applied to reduce the generation of false vectors. Individual vectors have been compared in a neighbourhood area (5×5 pixels size) and ones that deviate too much from their neighbours can be replaced by the average of the neighbours as a reasonable estimate of true velocities. This process has been performed for three iterations with an acceptance factor of 0.1. Additionally, a validation process was implemented to eliminate false samples by limiting the range of velocity values. In particular, all vector values exceeding 100 m/s were rejected.

4. Results and discussion

In order to obtain a comprehensive understanding of the velocity profile within the combustion chamber, an analysis of the tangential velocity component has been carried out using the PIV-velocity vector distribution. The analysis was performed along the horizontal and vertical diameters passing through the combustion chamber axis, and the results are presented in Figure 3 and Figure 4. The tangential velocity field was found to be slightly off-axis due to the outlet flow effect originating from the connecting duct. In particular, the tangential velocity component was about 20% higher along the horizontal diameter on the right side of the combustion chamber for each crank angle. However, this effect was negligible along the vertical diameter, resulting in a flow field that can be considered uniform within the chamber, except near the outlet zone. The plots indicate an increase in the swirling flow as the piston moves upwards, with maximum values observed at −30 CAD ATDC. The velocity profiles on the horizontal diameter showed that the outlet region had the highest tangential velocity of approximately 50 m/s, while the region on the left side showed values of about 40 m/s at −30 CAD ATDC. On the other hand, the velocity profiles on the vertical diameter showed almost the same intensity on both sides of the combustion chamber, confirming a roughly uniform distribution of the flow field inside the chamber, except near the duct that supplied air from the cylinder. No information about flow velocity has been extracted in correspondence of the injector. The velocity profiles also showed an increase in velocity from −50 to −30 cad ATDC, after which decrease in the velocity is expected in the periphery of the chamber because of the decrease in the piston speed.

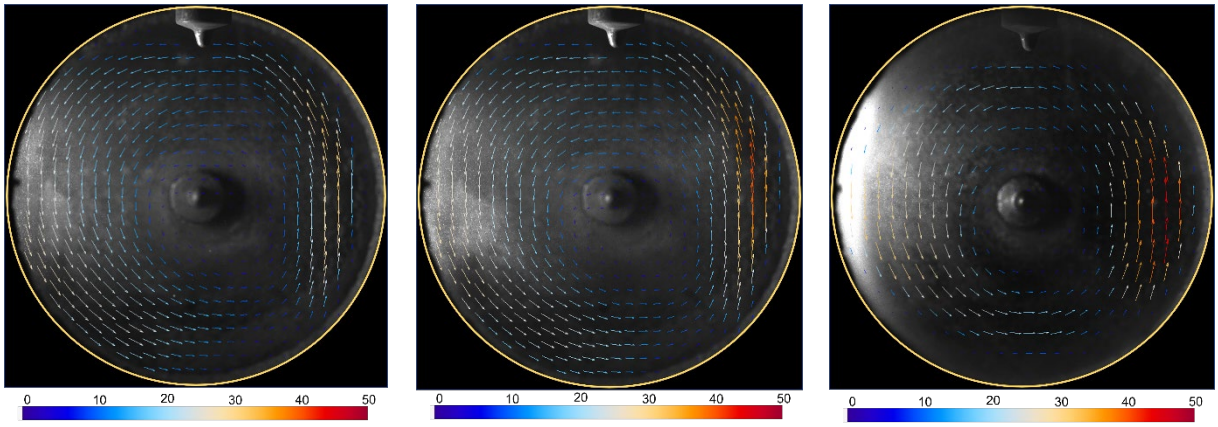

SOA = -50 CAD BFTDC **SOA = -40 CAD BFTDC** **SOA = -30 CAD BFTDC**

Figure 3. Ensemble-averaged air velocity vector fields at different crank angle before TDC.

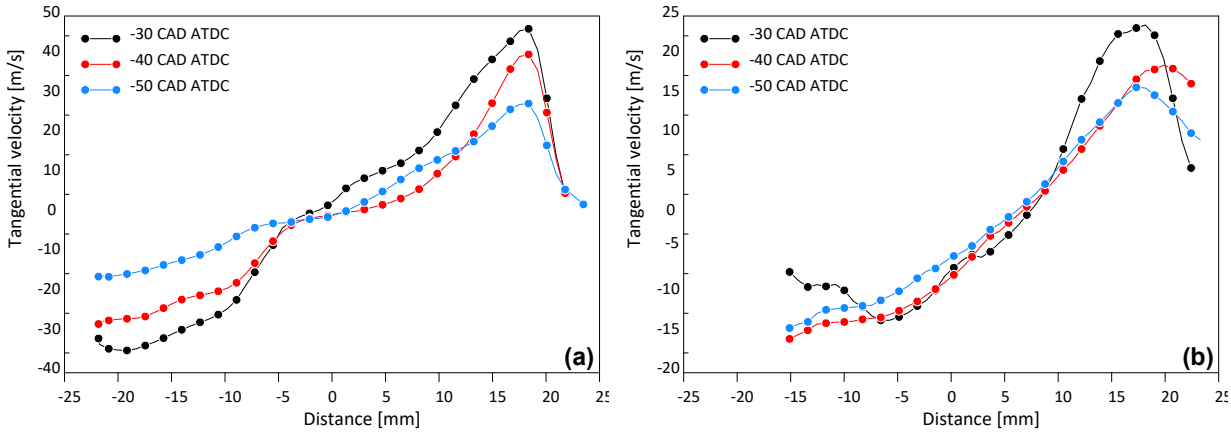

Figure 4. Air tangential velocity component on the horizontal (a) and vertical (b) diameters at different crank angles

Before performing the PIV analysis, a macroscopic characterization of the spray of water in the combustion chamber has been carried out. The plot of the tip penetration length is shown in Figure 5. Figure 6 represents the acquired images used for the characterization of the spray. The injection temperature was set to 300°C, the injection pressure to 30MPa and the start of injection to 10 CAD BFTDC. The tip penetration profile was similar to fuel common rail injection: first, an hydraulic injection delay of about 100 μs was observed, followed by an inflection point, indicating the droplets break-up occurrence, than spray propagates with an almost constant speed, resulting in linear chart. During this stage, the spray shows high momentum and compact growth, with relatively low air resistance despite the backpressure. The first water-air interaction effects become visible at the periphery of the spray, where shear stresses caused by air motion are observed. As injection progresses, the air brake effect becomes noticeable, with the spray no longer growing compactly and drops becoming dispersed, resulting in nearly stationary penetration. The swirling chamber effect also affects the curvature of the spray, which is more evident in the dispersed droplets, due to the combined effect of higher tangential air speed and the larger dilution of spray. In the following, the effects of the SCW injection strategy parameters on the airflow in the chamber are discussed.

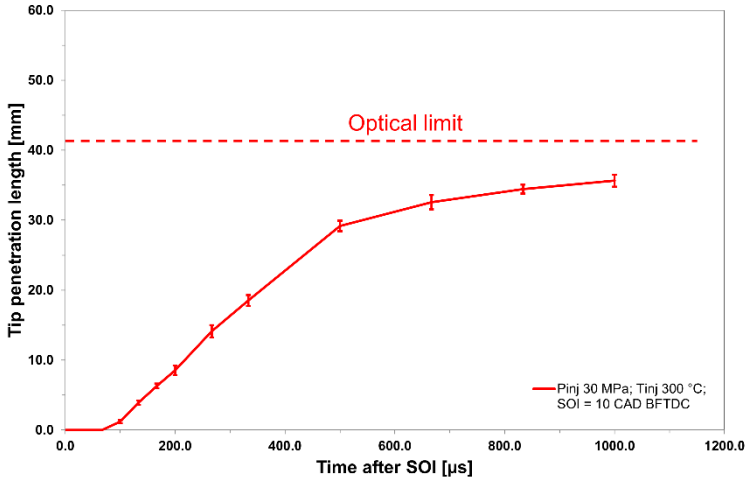

Figure 5. Water spray tip penetration length evolution (SOI = 10 CAD BFTDC, p_{inj} = 30 MPa, T_{inj} = 300°C).

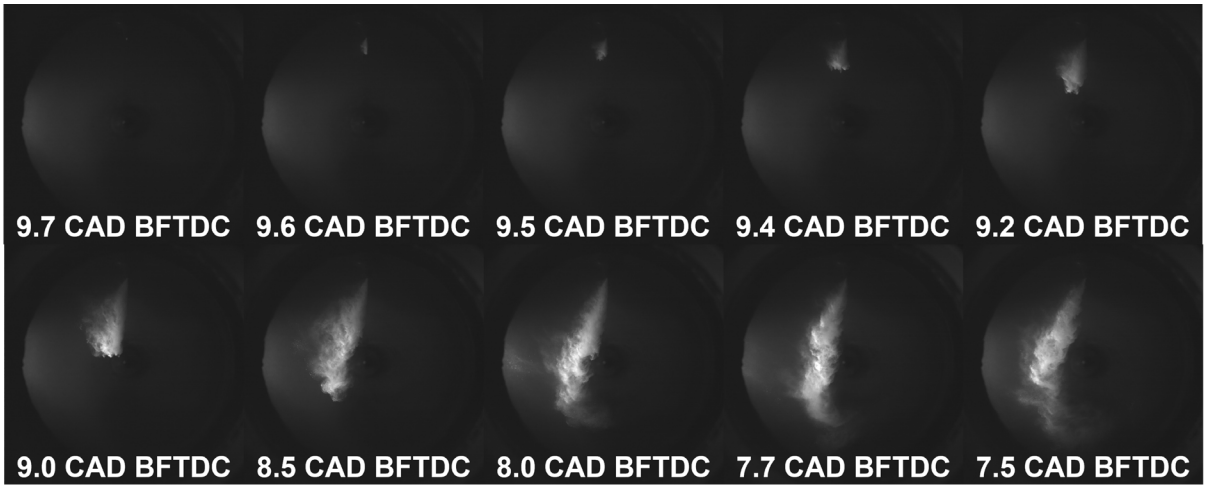

Figure 6. Water spray evolution (SOI = 10 CAD BFTDC, p_{inj} = 30 MPa, T_{inj} = 300°C).

4.1 Effects of injection pressure

The effects of injection pressure on the interaction between the spray and the airflow were evaluated by comparing the PIV results for tests with an injection temperature of 420°C, an injection start at top dead center (0 CAD ATDC), and an injection duration of 166 µs (0.5 CAD@500 rpm). Figure 7 reports the results of the averaged mean velocity vector distribution of the swirling air with the injected water and the vorticity distribution for two different injection pressures of 25 MPa and 30 MPa, respectively; the acquisition time was set at 2.1 CAD (700 µs) after the electronic injection command. From the analysis of the spray, the influence of the higher injection pressure (in the case of 30 MPa) is evident. Due to the larger momentum of the droplets, they are less affected by turbulence in the chamber, as evidenced by the lower curvature of the spray axis. This effect is confirmed by the analysis of streamlines of the air flow at the edge of the spray. In fact, the cutting effect on the sides of the spray is noted, which causes the water droplets removed from the spray to follow the swirl motion induced by the chamber geometry, and a deviation of the streamlines near the tip, where the droplets impact the air frontally. The maximum velocity of the flow field, about 42 m/s, was found in the region downstream of the spray, at the inlet of the tangential duct connecting the main cylinder to the optically accessible chamber. No significant effects on the vorticity of the flow field were observed.

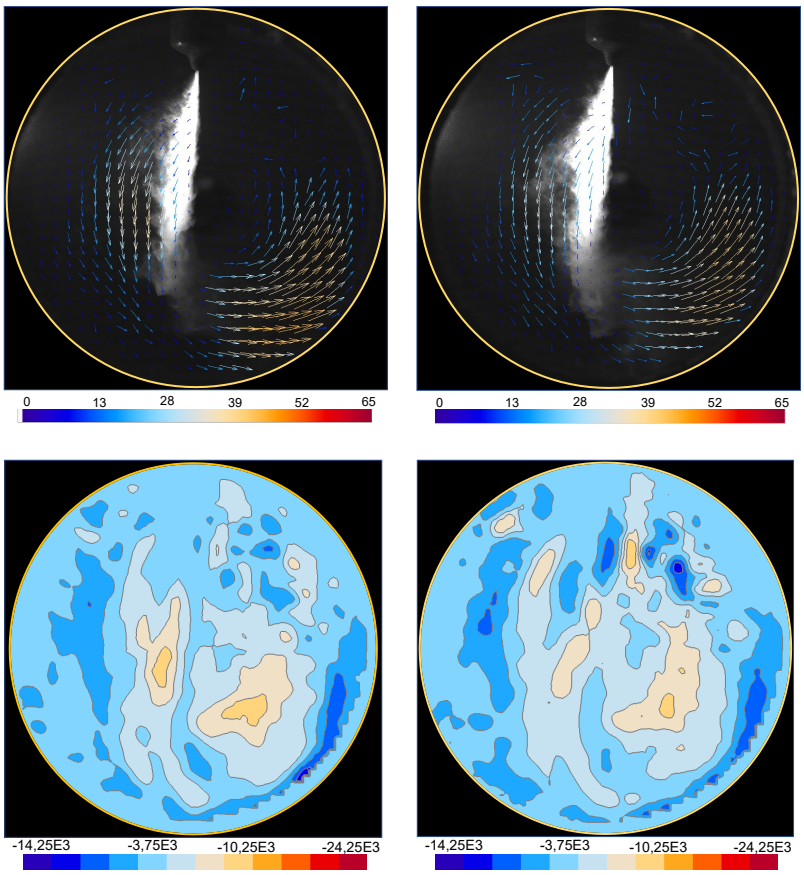

p_{inj} = 25 MPa **p_{inj} = 30 MPa**

Figure 7. Ensemble-averaged air velocity vector fields (m/s) and vorticity (1/s) distribution at SOA=1000 µs, T_{inj}=420°C, SOI=0 CAD BFTDC, and different injection pressures

4.2 Effects of injection temperature

Figure 8 shows the effect of temperature on spray characteristics through maps of the water-air interaction at three different injection temperatures: 400, 420, and 465°C, at an injection pressure of 25 MPa, for an injection duration of 166 µs. Injection starts at top dead center (0 CAD ATDC), and the acquisition time is 3 CAD (1000 µs) after the electronic injection command. The increase in temperature reduces the water density and momentum, resulting in a shorter liquid phase penetration length. The lower density and reduced momentum also increase the impact of combustion chamber air on the liquid jet core immediately after exiting the nozzle, resulting in an increase in cone angle, of 21°, 23° and 27°, respectively. As the temperature increases, a stronger interaction between the spray and air is observed in the lateral regions of the jet, where the shearing effect of the air on the spray with lower density and surface tension leads to a higher number of dispersed droplets in the combustion chamber. This effect is also confirmed by the increase in vorticity next to the spray. Conversely, the lower momentum at the tip reduces the axial penetration effect of the jet on the surrounding air, as evidenced by the lower deviation of the streamlines in the case of the highest injection temperature.

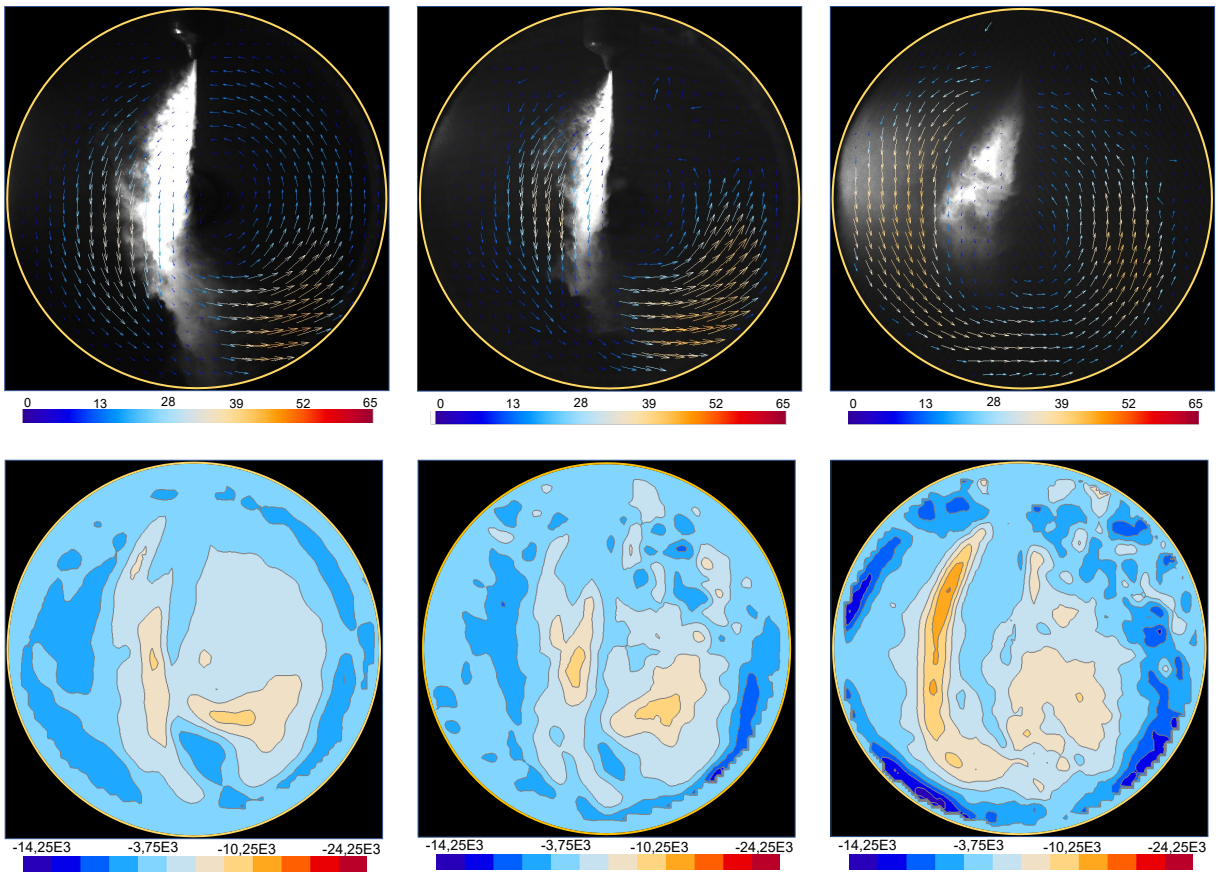

T_{inj} = 400 °C **T_{inj} = 420 °C** **T_{inj} = 465 °C**

Figure 8. Ensemble-averaged air velocity vector fields (m/s) and vorticity (1/s) distribution at SOA=1000 µs, p_{inj}=25 MPa, SOI=0 CAD BFTDC, and different injection temperatures.

4.3 Effects of injection timing

Figure 9 shows the PIV results at an injection pressure of 30 MPa, an injection temperature of 420°C, and an injection duration of 166 µs, for three different injection timings: 0, 10, and 20 CAD ATDC. By delaying the injection towards the expansion stroke, a reduction in the effect of induced turbulence in the combustion chamber on the spray morphology is observed. As the injection timing is further delayed, the penetration length of the jet increases, until it impacts the side wall of the pre-chamber; the dispersion of the spray in the chamber is strongly lower as evidenced by the smaller surface area occupied by the jet and the reduction in vorticity near the outlet duct. This behaviour is attributed to the reversal of swirl motion due to the expansion stroke of the piston in the main cylinder and the reduction of pressure in the combustion chamber.

Conclusions

In this study, the fluid dynamics during the injection of supercritical water were experimentally investigated in the combustion chamber of a 2-stroke Diesel engine, equipped with an injection system that allow independent regulation of injection pressure, temperature, duration, and timing. The experiments were carried out under different operating conditions to evaluate their effects on the fluid dynamics in the combustion chamber. First, the airflow velocity field was characterized at different engine crank angles, observing the evolution of air swirl motion, followed by a macroscopic characterization of the water spray at given injection temperature and pressure (300 °C, 30 MPa). The study also explored the interaction between supercritical water and air using PIV analysis, which

provided information on the spray morphology, tip penetration, and velocity vector distribution of the water droplets within the combustion chamber for different injection strategies. The results showed an increase in the spray-air interaction when both injection pressure and temperature increased. The cone angle of the spray increased with injection temperature, more in detail it was measured as 21°, 23° and 27° corresponding to temperatures of 400, 420, 465 °C, respectively. The stronger interaction of the spray with the air was also evident in the increase of the flow vorticity next to the spray. Moving the injection to the expansion stroke reduces the effects of supercritical water injection. In particular, reduced spray curvature and flow vorticity were observed, mainly due to the inversion of the piston motion and the reduction in chamber pressure.

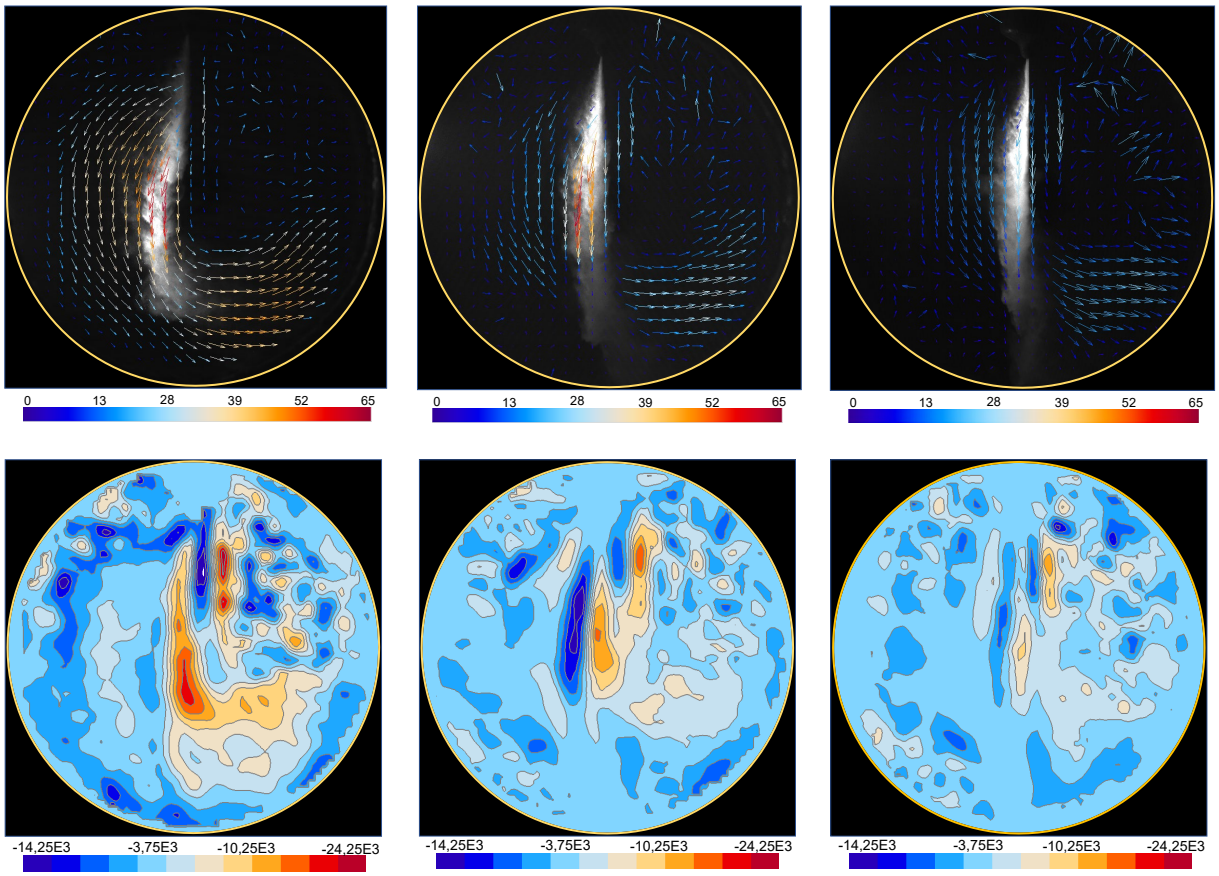

SOI = 0 CAD AFTDC **SOI = 10 CAD AFTDC** **SOI = 20 CAD AFTDC**

Figure 9. Ensemble-averaged air velocity vector fields (m/s) and vorticity (1/s) distribution at SOA=1000 μs, T_{inj}=430°C, p_{inj}=30 MPa, and different start of injection.

Acknowledgements
The authors thank Mr. Alfredo Mazzei for the technical support to the experimental campaign.

References

[1] Energy Agency I 2020 World Energy Outlook 2020
[2] Wang Y, Zu B, Xu Y, Wang Z and Liu J 2016 Performance analysis of a Miller cycle engine by an indirect analysis method with sparking and knock in consideration *Energy Convers Manag* **119** 316–26

[3] Luisi S, Doria V, Stroppiana A, Millo F and Mirzaeian M 2015 Experimental Investigation on Early and Late Intake Valve Closures for Knock Mitigation through Miller Cycle in a Downsized Turbocharged Engine *SAE Technical Papers* **2015-April**
[4] Li T, Gao Y, Wang J and Chen Z 2014 The Miller cycle effects on improvement of fuel economy in a highly boosted, high compression ratio, direct-injection gasoline engine: EIVC vs. LIVC *Energy Convers Manag* **79** 59–65
[5] Wang J, Duan X, Wang W, Guan J, Li Y and Liu J 2021 Effects of the continuous variable valve lift system and Miller cycle strategy on the performance behavior of the lean-burn natural gas spark ignition engine *Fuel* **297**
[6] Xie F, Hong W, Su Y, Zhang M and Jiang B 2017 Effect of external hot EGR dilution on combustion, performance and particulate emissions of a GDI engine *Energy Convers Manag* **142** 69–81
[7] Wei H, Feng D, Pan J, Shao A and Pan M 2017 Knock characteristics of SI engine fueled with n-butanol in combination with different EGR rate *Energy* **118** 190–6
[8] Zhao Z, Yu X, Huang Y, Shi W, Guo Z, Li Z, Du Y, Jin Z, Li D, Wang T and Li Y 2022 Experimental study on combustion and emission of an SI engine with ethanol /gasoline combined injection and EGR *J Clean Prod* **331** 129903
[9] Marchitto L, Tornatore C, Valentino G and Teodosio L 2019 Impact of Cooled EGR on Performance and Emissions of a Turbocharged Spark-Ignition Engine under Low-Full Load Conditions *SAE Technical Papers* **2019**
[10] Yin X, Li W, Zhang W, Lv X, Yang B, Wang Y and Zeng K 2022 Experimental analysis of the EGR rate and temperature impact on combustion and emissions characteristics in a heavy-duty NG engine *Fuel* **310**
[11] Mingrui W, Thanh Sa N, Turkson R F, Jinping L and Guanlun G 2017 Water injection for higher engine performance and lower emissions *Journal of the Energy Institute* **90** 285–99
[12] Hoppe F, Thewes M, Baumgarten H and Dohmen J 2015 Water injection for gasoline engines: Potentials, challenges, and solutions: *https://doi.org/10.1177/1468087415599867* **17** 86–96
[13] Li A, Zheng Z and Peng T 2020 Effect of water injection on the knock, combustion, and emissions of a direct injection gasoline engine *Fuel* **268** 117376
[14] Franzke B, Voßhall T, Adomeit P and Müller A 2019 Water Injection for Meeting Future RDE Requirements for Turbocharged Gasoline Engines *MTZ worldwide 2019 80:3* **80** 30–9
[15] Zhu S, Hu B, Akehurst S, Copeland C, Lewis A, Yuan H, Kennedy I, Bernards J and Branney C 2019 A review of water injection applied on the internal combustion engine *Energy Convers Manag* **184** 139–58
[16] Piras M, Teodosio L, Tornatore C, Marchitto L and Bozza F 2022 Exploring the potentials of water injection to improve fuel consumption and torque in a small displacement PFI spark-ignition engine *Fuel* **327** 125224
[17] Subramanian K A 2011 A comparison of water–diesel emulsion and timed injection of water into the intake manifold of a diesel engine for simultaneous control of NO and smoke emissions *Energy Convers Manag* **52** 849–57
[18] Zhao R, Zhang Z, Zhuge W, Zhang Y and Yin Y 2018 Comparative study on different water/steam injection layouts for fuel reduction in a turbocompound diesel engine *Energy Convers Manag* **171** 1487–501
[19] Abdelhameed E, Aoyagi T, Tashima H and Tsuru D 2021 PIV measurements of entrainment process of directly injected media in internal combustion engines *14th International Symposium on Particle Image Velocimetry* **1**
[20] Chraniotis A, Tourlidakis A, Tsiogkas V D, Chraniotis A and Kolokotronis D 2019 Cold Flow Measurement in Optical Internal Combustion Engine using PIV *13th International Symposium on Particle Image Velocimetry – ISPIV 2019*

[21] Valentino G, Allocca L and Marchitto L 2011 PIV Investigation of High Swirl Flow on Spray Structure and its Effect on Emissions in a Diesel-Like Environment *SAE 2011 World Congress and Exhibition*